von Karman Institute for Fluid Dynamics

Lecture Series 2025-01

MEASUREMENT, MODELLING AND SIMULATIONS TECHNIQUES FOR NOVEL AIRCRAFT ARCHITECTURES

November 4-6, 2024

UNDERSTANDING DIFFERENCES AND SIMILARITIES BETWEEN PROPELLER AND FAN NOISE BASED ON SIMPLIFIED MODELLING

S. Guérin
Deutsches Zentrum für Luft- und Raumfahrt e.V., Berlin, Germany

1 Introduction

The following notes serve to provide supplementary material to the lecture, entitled "Understanding Differences and Similarities between Propeller and Fan Noise Based on Simplified Modelling".

1.1 Engines used in passenger aircraft

As an introduction, we begin by looking at the two examples of commercial aircraft shown in Fig. 1. The first is a Dornier 328, and the second is an Airbus A350. The Dornier 328 can accommodate 35 passengers at a speed corresponding to a flight Mach number of $M_\infty = 0.54$, while the Airbus A350 can carry over 300 passengers at $M_\infty = 0.85$. The former is powered by two turboprop engines with a 6-blade propeller of 3.35 m diameter, while the latter uses two turbofans with a 22-blade fan of 3 m diameter. The choice of a turboprop rather than a turbofan is due to the very distinct characteristics of the two concepts. The final design involved many disciplines. It is the result of an iterative process aimed at economic viability, environmental impact (noise being a key factor) and technological feasibility.



Figure 1: (Left) Dornier 328-100, (right) A350-941 (photos: Tobias Lade).

A turboprop uses core exhaust energy to drive a propeller, which generates thrust. This type of engine is efficient at lower speeds and altitudes and is used on regional or commuter aircraft. A turbofan operates on a different principle. The upstream inlet reduces the velocity of the incoming air (at cruise) and converts it into pressure. The rotor, driven by the core, adds energy to the airflow. This results in an increase in total pressure. The stator converts the swirl behind the rotor into pressure. Finally, the nozzle converts the pressure into velocity. Turbofans are optimised for higher speeds and altitudes. They are used for commercial jetliners and long-haul flights.

Before getting to the heart of the matter, it's important to note that there is a range of possibilities, some of which, such as the very recent open fan, clearly attempt to combine the best of both worlds (see Fig. 2). With the advent of electric propulsion, especially in the field of UAMs, this spectrum is expanding to include distributed propulsion.

1.2 Objectives of the lecture

In this course our attention is focussed on the noise emitted by the propeller and the low-pressure fan stage of a turbofan, simply called the fan. The fan consists of a rotor

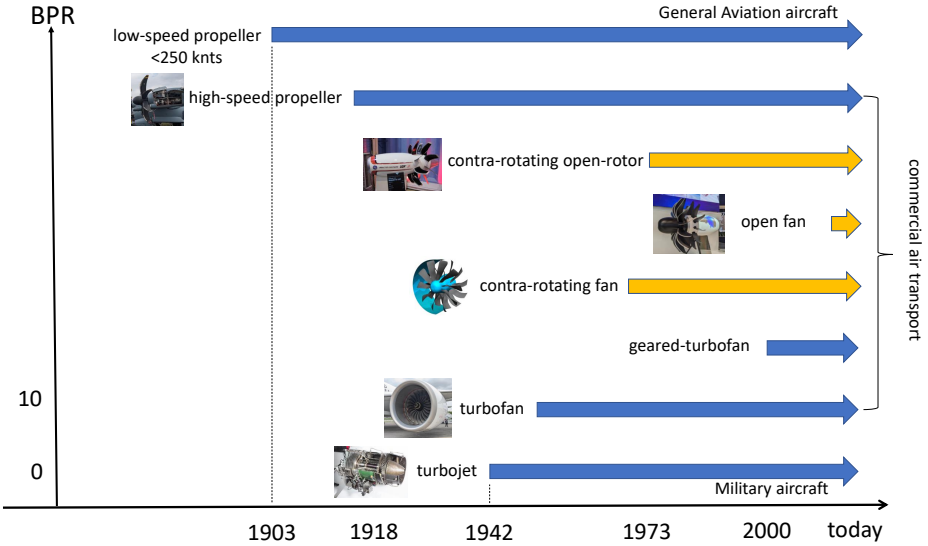


Figure 2: Engine concepts for fuel-powered aircraft.

and a stator enclosed in a nacelle. Other engine sources such as core and jet noise are not covered.

The performance of the two example engines shown above is very different. Obviously it would not be fair to compare them in terms of noise levels. In general, the comparative assessment of turboprop and turbofan aircraft is not straightforward due to the inherent differences in their respective advantages and disadvantages. Therefore, we prefer to focus on noise mechanisms, radiation efficiency, relative noise composition between tones and broadband, directivity, reduction methods, etc.

The differences and similarities in terms of geometry, aerodynamics and ultimately acoustics are examined in this review. Most of the results have been obtained using the code *PropNoise*, first developed during Antoine Moreau's PhD thesis (Moreau (2017)). Simplified models are used, based as much as possible on physics. In this document, priority is given to the results obtained at DLR in Berlin. Other studies are referred to in our publications.

2 Air-breathing propulsion

The aim of this section is to explain where the function of a propeller differs from that of a fan and how this affects the geometry and aerodynamic parameters that characterise them. This should help us to understand the differences in noise, as these are essentially the result of these parameters.

2.1 Thrust and propulsive efficiency

By applying the integral momentum theorem derived from Newton's second law (Spakovszky (2007)) to a control volume surrounding an air-breathing propulsion system as illustrated in Fig. 3, an equation for the thrust, T, is obtained:

$$T = \dot{m}(U_e - U_\infty), \tag{1}$$

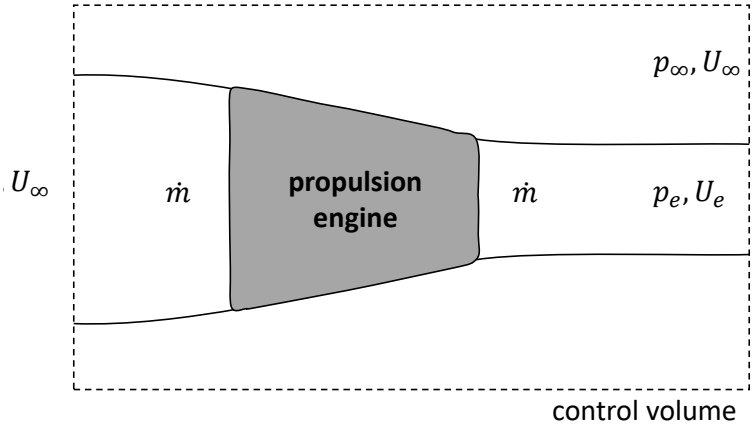


Figure 3: Air-breathing propulsion.

where it is assumed that the pressure at the control surface outlet is equal to the ambient static pressure, i.e. $p_e = p_\infty$. Eq. 1 indicates that thrust can be increased either by increasing the mass flow rate $\dot{m}$ or by increasing the difference between the exhaust velocity U_e and the flight velocity U_∞.

Moreover, a propulsive efficiency η_{prop} can be calculated. This represents the ratio between the propulsive power and the rate of production of kinetic energy. It reads:

$$\eta_{prop} = \frac{2}{1 + \frac{U_e}{U_\infty}}. \tag{2}$$

The previous equation shows that reducing the exit velocity improves propulsion efficiency. However, the effect on thrust is antagonistic.

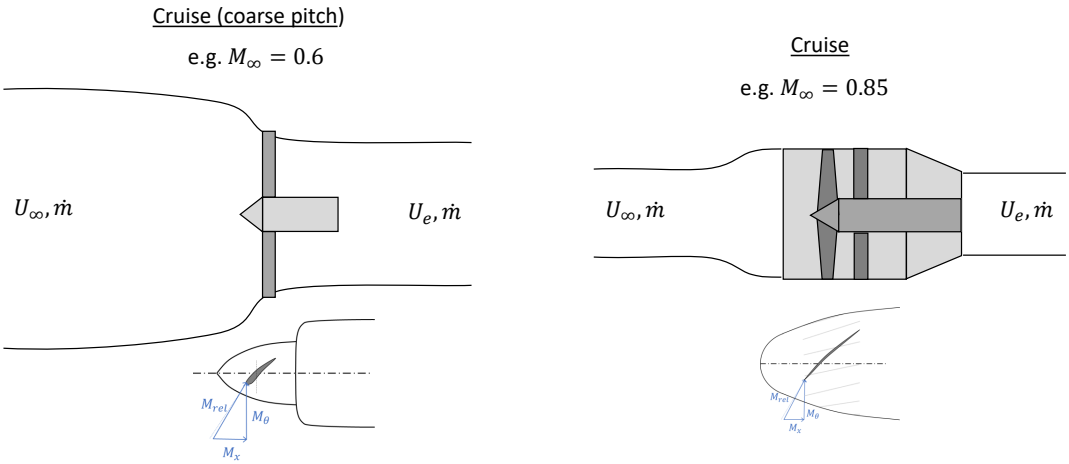


Figure 4: (left) Propeller and (right) fan propulsion at cruise.

2.2 Propeller versus fan propulsion

A propeller operates at a relatively low specific thrust ($T/\dot{m}$). This means that a large volume of air is displaced at relatively low speeds. Consequently, a propeller operates at

low disk loading. This provides an explanation for the large diameter of the propeller, among other differences. In the absence of a nacelle, the axial speed upstream of the propeller is imposed by the forward speed of the aircraft (see Fig. 4). As will be indicated subsequently, it is crucial that the propeller rotates at subsonic speed, i.e. with a relative tip speed below one. These two factors limit the maximum forward speed an aircraft equipped with turboprops can achieve. Furthermore, for optimal efficiency, the propeller must be equipped with a variable pitch system to guarantee that the flow is at the suitable angle relative to the blades.

The fan of a turbofan, on the other hand, compresses the flow. It displaces a "smaller" volume of air, but expels it at a higher speed (the specific thrust is therefore greater). This allows the aircraft to move faster, but also results in a much more compact engine. To achieve this result, the fan must have other characteristics, as we shall see. In a fan stage, the rotor is followed by a stator that straightens the flow. This is not the case with a propeller, which creates a swirl downstream. It is also important to note that the nacelle regulates the flow upstream of the fan: it accelerates the flow at take-off and decelerates it at cruise. This is why conventional fans do not need a variable pitch system.

3 Rotor aerodynamics

The example of the two engines at the beginning showed that a propeller and a fan can be very different in terms of number of blades, Mach number, etc. This section aims to explain some of the main reasons for this. In fact, the noise generated by a rotor can be modelled based on its geometric and aerodynamic characteristics.

3.1 Propeller blade forces

The aerodynamic performance of a propeller is frequently modelled using the blade element momentum theory, which combines the momentum theory previously described, in which the propeller is replaced by a disc actuator, with the blade element, in which a blade is divided into two-dimensional segments on which a lift force L and a drag force D act. The thrust T is the projection of these forces along the axis of the motor. The moment Q called torque is defined by multiplying the force applied in the plane of rotor rotation by the radial position. Normalised to the upstream speed and density, these forces vary as a function of the inflow incidence, Reynolds number and Mach number.

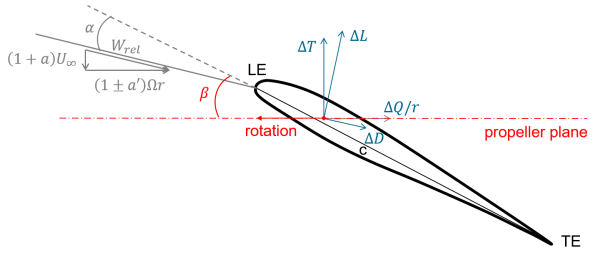


Figure 5: Force components acting on a rotating blade.

3.2 Flow turning, fan pressure ratio and blade solidity

Since the main role of a fan is to compress the air passing through it, it is useful to understand how the fan pressure ratio $FPR = Pt_B/Pt_A$, which is the ratio of the downstream total pressure to the upstream total pressure, is related to the two parameters that are the rotational speed U and the flow turning $\Delta W_\theta = (W_{\theta,A} - W_{\theta,B})$ (see Fig. 6). The connection is made via the total enthalpy increase ΔH_t produced by the rotor:

$$\Delta H_t = U \cdot \Delta W_\theta = c_p T_{t,A} \frac{FPR^{\frac{\gamma-1}{\gamma}} - 1}{\eta_{ise}}, \tag{3}$$

where η_{ise} is the isentropic efficiency. This expression shows that it is possible to increase the pressure in two ways: by increasing the speed of the rotor and/or by increasing the flow turning.

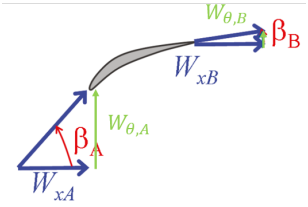


Figure 6: Flow vector components up- and downstream of a rotor blade.

3.3 Relation between lift, flow turning and solidity

The flow turning, the blade lift coefficient C_L and the solidity σ can be related as follows (Moreau (2017)):

$$C_L = \frac{2\Delta W_\theta}{\sigma W_m}, \tag{4}$$

where W_m is a mean value between the velocity upstream and downstream of the blade in the rotor frame. This equation shows that increasing the solidity, defined as the chord-to-pitch ratio, is a good way of increasing the flow turning. The next expression shows that you need to increase the number of blades and/or lengthen the chord in order to increase solidity:

$$\sigma = \frac{c}{s} = \frac{B \cdot c}{2\pi r}. \tag{5}$$

In fact, the number of blades is determined by optimum aerodynamics. Too few blades can lead to aerodynamic overloading of the rotor (with the risk of flow separation), whereas too many blades can increase losses. Weight and structural constraints also play a role.

3.4 Aerodynamic of isolated airfoils and cascade

On the left of Fig. 7 we look at the effect of the angle of incidence on an isolated airfoil. This result shows that as the angle of incidence of the airfoil increases, the separation point shifts upstream. The lift increases linearly with the angle of attack until stall is reached, resulting in a drop in lift and a rapid increase in drag losses. The flow is

completely separated on the suction side. The variation in loading is accompanied by a variation in wake characteristics. The more the profile is loaded, the thicker the boundary layer and the wider and more turbulent the wake. In the case of interaction with a downstream component (e.g. the stator of a fan or the wing downstream of the propeller), this has a very important effect on the noise amplitude. This example illustrates the close relationship between aerodynamics, unsteady aerodynamics and noise generation.

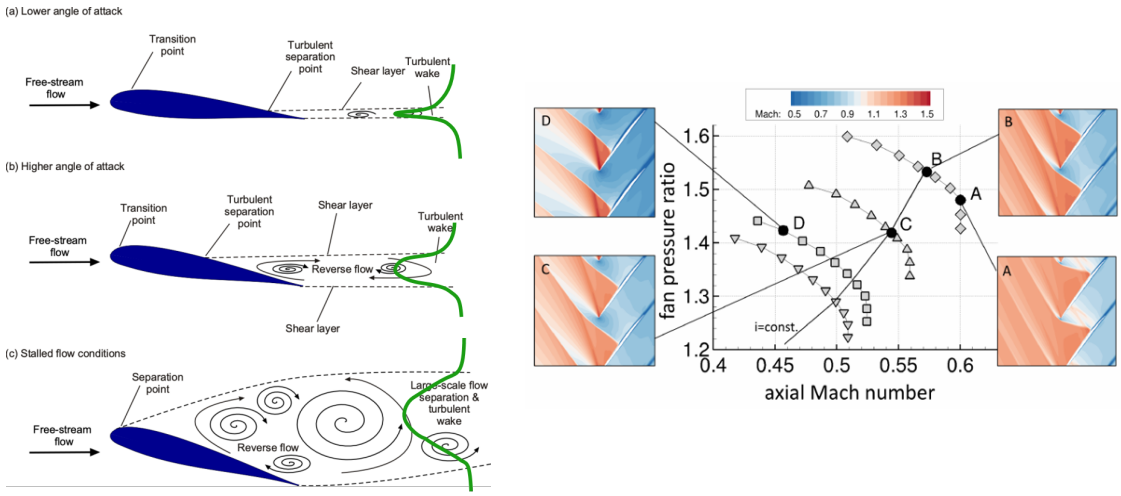


Figure 7: (left) Airfoil wake for different values of angle of attack (Picture reproduced from *Introduction to Aerospace Flight Vehicles. ISBN 979-8-9852614-0-0* © *2022–2024 by J. Gordon Leishman - Leishman_ebook@erau.edu* - and enhanced with wakes). (right) Shocks in a 2D rotor cascade (Copyright by Moreau, Staggat, Gscheidle (2019). Reproduced with permission).

The appearance of shocks at high speeds changes the situation since an isolated airfoil becomes very inefficient: lift drops and losses increase very rapidly. Therefore, from an aerodynamic point of view, it is better to avoid this area for a propeller. On the contrary, cascades of airfoils with supersonic inflow are efficient to increase the pressure across a fan. As shown in the right-hand side of Fig. 7, the flow downstream of the shocks is subsonic downstream of a cascade. In addition, cascades can handle higher aerodynamic loads by controlling the boundary layer and reducing flow separation. The choice of cascade design and the selected Mach number represent a compromise between pressure rise and loss.

For low speed propellers, thicker profiles are preferred as they are more robust to variations in angle of attack. Blades for high speed turbofans are thin, i.e. with low thickness and low camber to reduce losses. These profiles are more sensitive to changes in angle of attack.

4 Rotor acoustics

With the knowledge gained from the previous sections, we can now turn to the acoustic part of this study. We are interested in the theoretical description of noise generation based on the aeroacoustic analogy. In the subsonic regime it is possible to apply this

analogy with some confidence. A simplified version is presented which allows propeller and fan cases to be compared on the same theoretical basis.

Firstly, the Green's function is introduced. This is different for a source in the free field and one enclosed in a duct. Both solutions are formulated in the frequency domain and decomposed into azimuthal components. By retaining the same formalism, it is possible to highlight the similarities and differences between the two problems. The issue of radiative efficiency is then discussed in detail, as it plays an essential role. The study is extended to transmission effects in a duct, and the question of radiation at the ends of a duct is quickly addressed.

Secondly, the solution to the aeroacoustic analogy is simplified by assuming a thin blade profile. In this case, it is possible to describe the source terms common to the propeller and fan cases in a simple way.

Thirdly, we briefly consider the case of the blade response function, which plays a special role in predicting the unsteady lift induced by a gust hitting a blade.

4.1 Sound sources

The different sources of noise emitted by an isolated propeller and an isolated fan, i.e. without considering the installation effect, are listed in Table 1 and shown in Fig. 8.

Source	**Mechanism**	**Spectral content**	**Propeller**	**Fan**
rotor noise	steady loading steady thickness st. potential flow	tonal	yes	cutoff for $M_{trel} < 1$
	shocks	multiple tones	no	for $M_{trel} > 1$
airfoil self-noise	trailing-edge turb. scattering	bbn	yes	yes
inflow→rotor interac. (a.o.a or atmos. turb.)	unsteady loading	bbn+tonal	yes	yes
rotor→stator interac. (wakes + tip vortex)			no	yes
rotor←stator interac. (potential field)		tonal	no	yes

Table 1: Sound sources for an isolated propeller and fan stage.

4.2 Modelling approach based on the aero-acoustic analogy

The aero-acoustic analogy, which was first proposed by Lighthill, is employed in this analysis. According to Goldstein (1976), it can be shown that the noise generated by a blade can be understood and modelled using the following equation:

$$p(\mathbf{z},t) = \frac{1}{T_{ref}} \int_{-\infty}^{\infty} \left(- \iint \left[\rho_0 W_n \frac{DG}{Dt_s} + f_i \frac{\partial G}{\partial z_{si}} \right] d^2 z_s + \iiint T_{ij} \frac{\partial^2 G}{\partial z_{si} \partial z_{sj}}) d^3 z_s \right) dt_s, \quad (6)$$

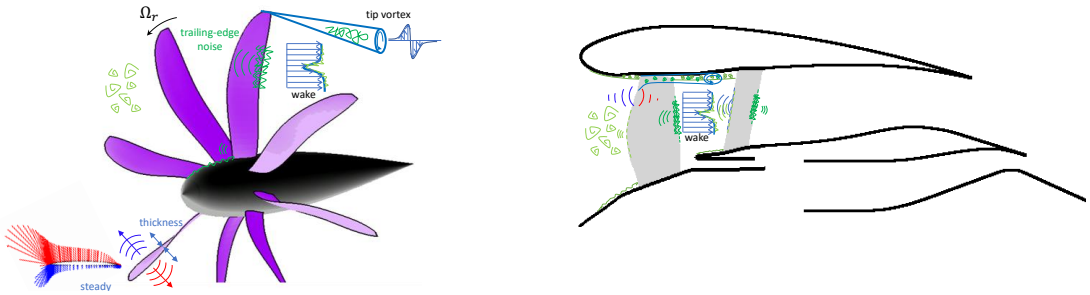


Figure 8: Aerodynamic sound sources for a propeller and a fan stage.

where $(\mathbf{z}, t)$ is the position and time of the observer and $(\mathbf{z_s}, t_s)$ is for the source. In this equation the first term describes a monopole emission. In the context of rotor noise, it corresponds to a volume displacement and is called thickness noise. The second term is a dipole and corresponds to the noise emitted by a force on a surface. The final term is a volume source. It represents a quadrupole associated with the Lighthill stress tensor. The function G represents a point-input response function called Green's function.

4.3 Green's function

4.3.1 Green's function in free field

We consider a source in an unbounded medium with a uniform, subsonic, axial flow. The solution for a harmonic source of radian frequency ω is given by

$$G^{\omega}(\mathbf{z}|\mathbf{z_s}) = \frac{e^{-ikR_e}}{4\pi R^*}, \tag{7}$$

where $k = \omega/c_0$ is a wavenumber, R^* is some distance equal to the source-observer distance $\rho = |\mathbf{z} - \mathbf{z_s}|$ for zero mean flow velocity. As shown by Moreau and Guérin (2011), this expression can be simplified in the far field and expressed in terms of the azimuthal component m using the Jacobi-Anger expansion. One defines the function g_m^{ω} such as

$$g_m^{\omega}(x, r|r_s) \approx i^m e^{-i(k_x x + k_r r)} \frac{1}{4\pi\rho} \frac{J_m(k_{r\theta} r_s)}{\sqrt{1 - M^2 \sin^2\psi}}. \tag{8}$$

The wavenumbers k_x and k_r are the axial and radial wavenumbers, respectively. $k_{r\theta}$ is called the combined radial-azimuthal wavenumber, M is the axial Mach number, and ψ the polar angle. The last term in Eq. (8) is identified as $\hat{g}_m^{\omega}$:

$$\hat{g}_m^{\omega}(\rho, \psi, |r_s) = \frac{1}{4\pi\rho} \frac{J_m(k_{r\theta} r_s)}{\sqrt{1 - M^2 \sin^2\psi}}. \tag{9}$$

The properties of the Bessel function J_m are such that its maximal amplitude decreases with the order m. Moreover, J_m takes small values when $k_{r\theta} r_s < |m|$ for all $m \neq 0$. As shown by Moreau (2017) for a rotating source, this condition is equivalent to $M_{rel} < 1/\sin\psi$. This means that for subsonic rotors in free field, low radiation efficiency and strong directional characteristics can be expected.

4.3.2 Green's function for an infinitely long circular duct

For an infinitely long, circular, hollow duct traversed by a uniform flow, each azimuthal component is expressed as a sum of discrete radial components n. Using the same notation as previously, Moreau and Guérin (2011) derived the following expression for g_m^ω:

$$g_m^\omega(x, r|r_s) = i \sum_{n=0}^{\infty} \frac{J_m(k_{r\theta} r)}{\sqrt{F_{mn}}} e^{-ik_x x} \hat{g}_{m,n}^\omega(r_s), \tag{10}$$

with

$$\hat{g}_{m,n}^\omega(r_s) = \frac{1}{4\pi R} \frac{J_m(k_{r\theta} r_s)}{kR\alpha_{mn}\sqrt{F_{mn}}}. \tag{11}$$

In this equation $k_{r\theta}$ now takes discrete solutions depending on (m, n). This is also the case for the axial wavenumber k_x, since both are related by the dispersion relation. In addition, k_x depends on the Mach number and the direction of propagation ($\pm$). Notice the similarities between Eq. (9) and (11).

In the above equation, the cut-on factor α_{mn} has been introduced:

$$\alpha_{mn} = \sqrt{1 - (1 - M^2)\left(\frac{k_{r\theta,mn}}{k}\right)^2}. \tag{12}$$

This factor is very important in duct acoustics. Indeed, the sound pressure is given by

$$p_{mn}^\omega(x, r, \theta, t) = A_{mn} f_{mn}(r) e^{i(k_{x,mn}^{\pm} x + m\theta - \omega t)}, \tag{13}$$

with A_{mn} the modal amplitude, f_{mn} a normalised Bessel function and

$$k_{x,mn}^{\pm} = \frac{k}{\beta^2}(-M \pm \alpha_{mn}). \tag{14}$$

So if the α_{mn} factor is imaginary, the axial wavenumber has an imaginary part, which explains the exponential axial decay of the sound pressure. For a mode to propagate over a long distance, α_{mn} must be real. In this case the mode is said to be cut-on. For each mode (m, n), there is a cut-off frequency f_c. An example of the pressure field of a spinning mode at (left) cut-off and (right) cut-on conditions is shown in Fig. 9.

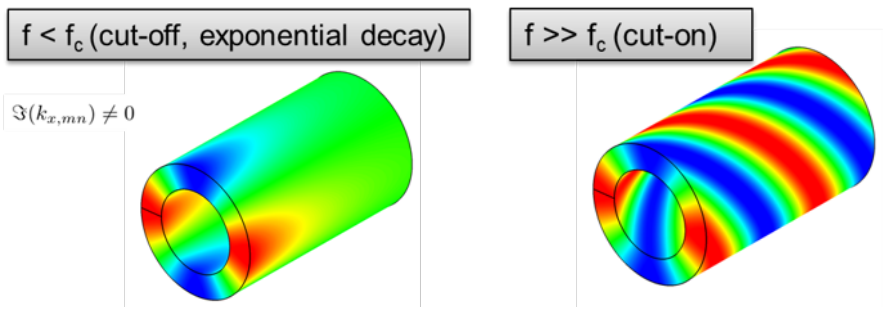


Figure 9: Example of mode propagation in duct (Copyright by Guérin (2017). Reproduced with permission.)

4.3.3 Radiation efficiency of azimutal modes

The results shown in Fig. 10 come from a study carried out by Moreau and Guérin (2011). They were obtained for a harmonically pulsating monopole placed at a position $r_s/R = 0.6$ in a duct and at an equivalent position in free field. This monopole induces an acoustic field, which is rich in azimuthal modes. The sound power amplitude of each mode (zero for cut-off modes) depends on the Helmholtz number kR and mode order m. If we consider a particular mode $m_0 = 5$, we see that its acoustic power decreases rapidly below the limit $kr_s = m_0$. In the channel, the cut-off effect is brutal and certain peaks appear each time a new radial mode is cut off. At high frequencies, the two solutions move closer together, as if the duct no longer played a role. The cut-off effect is also very clear in the results of the right plot, which shows the azimuthal modal content for $kR = 50$.

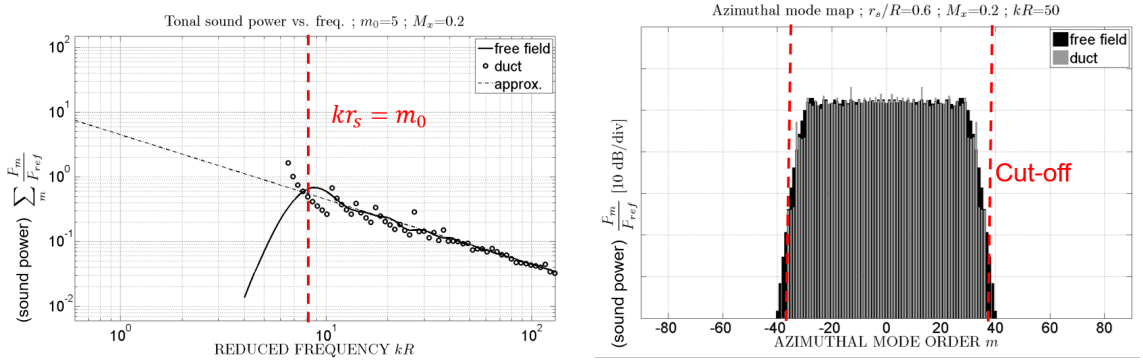


Figure 10: Acoustic radiation efficiency of a monopole source (Copyright by Moreau, Guérin (2011). Reproduced with permission.)

4.3.4 Wavenumbers

As can be seen in Table 2, the various wavenumbers introduced earlier can be expressed in a similar form. In the duct problem, the observer polar angle ψ has to be replaced by the modal energy propagation angle ψ_{mn}.

in free field	**in-duct config.**
$k_x = \frac{k}{\beta^2}\left(-M + \frac{\cos\psi}{\sqrt{1-M^2\sin^2\psi}}\right)$	$k^{\pm}_{x,mn} = \frac{k}{\beta^2}\left(-M + \frac{\cos\psi^{\pm}_{mn}}{\sqrt{1-M^2\sin^2\psi^{\pm}_{mn}}}\right)$
$k_{r\theta} = k\frac{\sin\psi}{\sqrt{1-M^2\sin^2\psi}}$	$k_{r\theta} = k\frac{\sin\psi^{\pm}_{mn}}{\sqrt{1-M^2\sin^2\psi^{\pm}_{mn}}}$
$k_\theta = m/r$	$k_\theta = m/r$
$k_r \approx k_{r\theta}$ for $r > \lvert m\rvert$	$k^2_{r\theta} = k^2_r + k^2_\theta$

Table 2: Solutions of the wavenumbers ($\beta^2 = 1 - M^2$).

4.3.5 Transmission and radiation

Chapman (1994) has shown mathematically that in the limit of high frequencies the propagation of a spinning mode (m, n) can be replaced by that of a ray whose trajectory is

piecewise linear. This approach allows an intuitive representation of things. Moreau (2020), based on Moreau et al. (2009), used this theory to model the transmission of acoustic waves through a cascade. (Mode and frequency scattering were ignored.) There is a significant masking effect of the interaction noise radiated forward by a transonic fan. This depends on the direction of rotation of the mode (co-rotating modes are better transmitted). Furthermore, the shielding effect increases rapidly at high speed (at supersonic speed, a wave can no longer travel up the flow).

In addition, Rice et al. (1979) have shown that the far-field directivity peak of a spinning mode emitted at the end of a duct corresponds to the angle of propagation of the acoustic energy of the mode in the duct. While at high frequency the power is fully transmitted to the outside, it tend to zero near the cut-off frequency. Guérin (2017) also showed that cut-off modes tends to radiate proportionally less the further they are from the cut-on limit.

4.4 Aero-acoustic analogy for "flat plate"-like airfoils

4.4.1 Simplified solution

We assume that the blades are thin and little cambered. This allows us to model each blade as an approximation of an infinitely thin flat plate. We define a direction l parallel to the chord and a direction n normal to the chord as shown in Fig. 11.

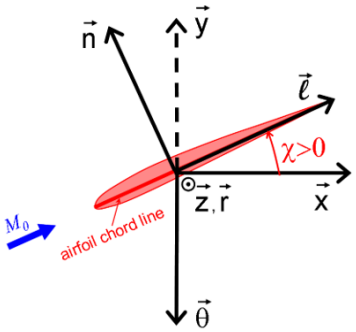


Figure 11: Flat plate approximation (Copyright by Moreau, Guérin (2011). Reproduced with permission.)

If we further assume that the blades do not interact with each other and are all identical and equidistant, it is possible to simplify the aero-acoustic analogy and replace it by a simple integral along the radius of Green's function multiplied by a source term σ_s as given in Table 3. In the case of tonal noise, a phase term set at the leading edge is added.

propeller	$p_m^\omega = e^{i(k_x x + k_r r)} B \int_{R_h}^{R_t} \hat{g}_m^\omega e^{-i(k_x x_{LE} + m\theta_{LE})} \sigma_s dr_s$
fan	$A_{mn}^{\omega,\pm} = B \int_{R_h}^{R_t} \hat{g}_{mn}^\omega e^{-i(k_x x_{LE} + m\theta_{LE})} \sigma_s dr_s$

Table 3: Simplified solution for B thin airfoils.

4.4.2 Source terms

The source terms can then be described as follows (Moreau and Guérin (2011), Moreau (2017)):

$$\begin{aligned}
\text{thickness noise:} \quad & \sigma_T = k_l^2 \int_{l=0}^{c} \rho_0 W_0^2 t(l) e^{ik_l l} dl \\
\text{lift noise:} \quad & \sigma_L = ik_n \int_{l=0}^{c} f_L^{\tilde{\omega}}(l) e^{ik_l l} dl \\
\text{drag noise:} \quad & \sigma_D = ik_l \int_{l=0}^{c} f_D^{\tilde{\omega}}(l) e^{ik_l l} dl \\
\text{quadrupole noise:} \quad & \sigma_Q = k_l^2 \int_{l=\infty}^{\infty} \int_{n=\infty}^{\infty} \rho_0 u_l^2(l,n) e^{i(k_l l + k_n n)} dn dl
\end{aligned}$$

Table 4: Definition for the various possible source terms σ_s.

A similar formulation exists for broadband noise. In free field, the solution is:

$$\langle {p_m^\omega}^2 \rangle = B \int_{R_h}^{R_t} |\hat{g}_m^\omega|^2 \langle \sigma_s^2 \rangle l_r dr_s. \tag{15}$$

The operator $\langle \cdot \rangle$ describes the expectation and l_r is a radial correlation length of the source. Sources of broadband noise are listed in Table 1.

4.4.3 Airfoil unsteady lift induced by vortical perturbations

One of the main sources of fan noise is produced by the interaction between the rotor wakes and the stator. This phenomenon is known as rotor–stator interaction noise. To determine this source, we need to be able to calculate the unsteady lift created by a gust hitting the stator vane. The simplest solution was proposed by Sears (1941) for a flat plate hit by a one-dimensional harmonic gust in a low Mach number flow. Another popular solution, valid at high frequencies for two-dimensional gusts, was proposed by Amiet (1975).

In fact, there are many theories that allow more complexity to be taken into account, as it is admitted that certain effects such as sweep, thickness and camber have a non-negligible effect on the solution.

There is also a cascade effect for high-solidity blade rows. In this case, the strong interaction between the blades makes it impossible to treat them as isolated. This effect is quite difficult to model. Studies (see e.g. Cheong et al. (2006)) have shown that there is a cut-off frequency below which a gust hitting the cascade does not efficiently radiate.

5 Some applications

5.1 Tonal noise

5.1.1 Blade passing frequency and azimuthal mode order

If all the blades are equal, the frequency of the tones emitted by a rotor at subsonic speed is given by

$$f_h = hBf_{rot}, \tag{16}$$

where f_h is the blade passing frequency (BPF) and f_{rot} is the rotor rotation frequency in Hz. The tone obtained for $h = 1$ is called the fundamental, and the other tones for $h > 1, \forall h \in \mathbf{N}$, are the harmonic tones. For the Dornier 328, the fundamental BPF of the propeller at take-off was approximated to be 140 Hz, while for the Airbus A350 the fundamental BPF emitted by the fan is 990 Hz, a much higher frequency.

The azimuthal modes of the rotor-locked tones m_{rotor} are equal to the number of rotor blades times the integer h:

$$m_{rotor} = hB. \tag{17}$$

In our examples we get $m_{rotor,bpf} = 6$ (resp. 22) for the propeller (resp. fan). These modes are not efficiently radiated at subsonic speeds.

For fans, the modal content of the acoustic field generated by the rotor–stator interaction is given by the modal spectrum (m_{rotor}) of the upstream velocity disturbance enhanced by the number of stator vanes (Tyler and Sofrin (1962)). The modal structure of the resulting acoustic periodic field is sparse and reads:

$$m_{rsi} = m_{rotor} \pm kV, \tag{18}$$

where $k \in \mathbf{N}^*$ and V is the number of vanes (again assumed to be equal). At BPF we have $m_{rsi} = \{\cdots -74, -26, 66, \cdots\}$. All these modes are cut-off at subsonic rotor tip speed. We can conclude that the A350 has a so-called cut-off design of the BPF tone.

5.1.2 Rotor-locked tones

For a propeller, the amplitude of the tonal noise is high, mainly because the steady loading and thickness sources are not perfectly cut-off in free field, as we explained earlier. The maximum noise is radiated vertically, as shown in the left part of Fig. 12 for the example of a propeller at take-off. The directivity is similar to the case of a cut-off mode radiated at the inlet or outlet of the duct.

There is an strong drop in the radiative efficiency of a spinning acoustic mode below its critical frequency as shown in Fig. 10. The figure on the right shows the behaviour of rotor-locked sources in the free field as a function of relative tip Mach number (Moreau (2017)). The noise increases much faster than the classical scaling law such as $PWL \propto 10\log(M^{5-6})$, which applies to cut-on sources. This is due to the radiative efficiency of the cut-off acoustic modes m_{rotor}, which varies strongly with M. The trends are different for each source mechanism because of the evolution of the source amplitude, but also because of the dependence on k_l and k_n. The latter explains why the thickness noise becomes as important as the lift noise at high Mach number, while the aerodynamic excitation pressure (not shown here) of the two sources evolve almost in parallel. The increase in the quadrupole term near the critical Mach number is due to the sudden increase in the corresponding source term.

For a fan, the sudden cut-off effect of the acoustic modes associated with the rotor inside the nacelle in the subsonic regime leads to an exponential decrease in this sound pressure in the axial direction. In addition, the radiative efficiency of this mode at the end of the duct is reduced, as we saw earlier. The nacelle is therefore an extremely effective means of cancelling this source.

However, in the transonic regime, i.e. when the speed at the blade tip is supersonic, the shocks generated at the fan propagate upstream into the intake. This propagation

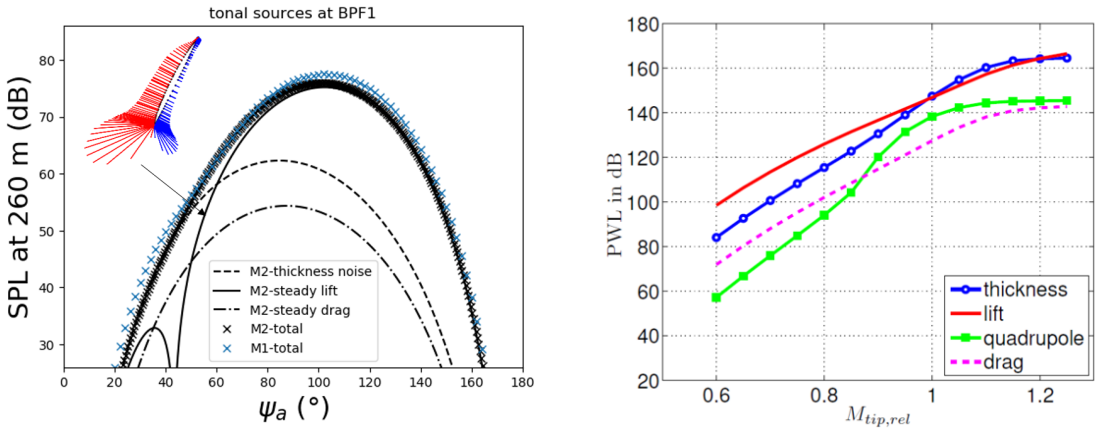


Figure 12: (left) Rotor tonal self-noise for a propeller during take-off ($B = 5$, $M_\infty = 0.167$, $M_{\theta,tip} = 0.167$) (Copyright by Guérin, Tormen (2023). Reproduced with permission.). (right) Acoustic trend of rotor-locked tones (Copyright by Moreau (2017). Reproduced with permission.).

is characterised by a merging of shocks due, among other things, to imperfections in the blade manufacturing process (see Fig. 13). This noise, known as buzz saw noise, is characteristic at take-off. Buzz saw noise is not a new rotor-locked stationary source, it is simply a change of state due to the transition from linear to non-linear behaviour with the formation of shocks. The aero-acoustic analogy is therefore no longer applicable in this case because of the non-linear effects.

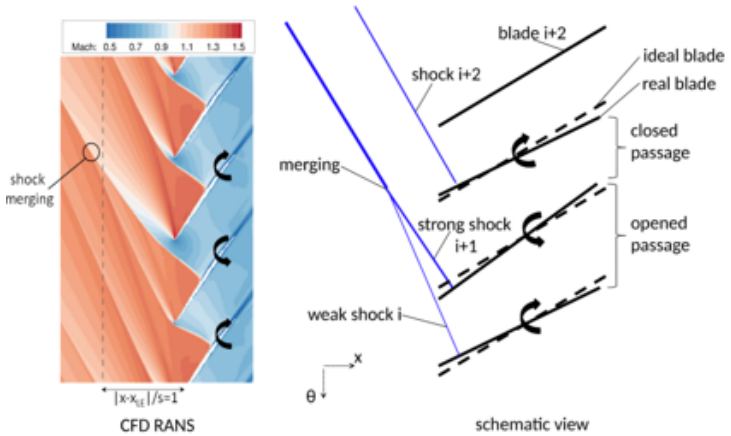


Figure 13: Shock merging as a result of small stagger angle variations (Copyright by Moreau, Staggat, Gscheidle (2019). Reproduced with permission.).

5.1.3 Rotor–stator interaction

For a fan, another source of tonal noise is the interaction between the rotor wakes and the stator blades. Each wake represents a mean velocity disturbance that can be modelled by a Gaussian function. We have seen from the A350 example that by choosing an appropriate

combination of rotor and stator blades, it is possible to induce an acoustic field that is acoustically cut-off, effectively helping to attenuate the tonal source of the rotor–stator interaction. This technique works for the BPF and possibly its first harmonic, i.e. 2×BPF, at low speed.

The cut-off mode technique is not applicable to the broadband noise component generated by the interaction of the wake and tip turbulence with the stator vanes. This is because the spectrum of the azimuthal components of the turbulence velocity field is broad and rich. Only by reducing the wake turbulence and/or the number of vanes can this source be effectively reduced. Fig. 14 shows the results of a benchmark performed as part of a European project to predict the broadband noise emitted by a fan. Only the rotor–stator interaction was predicted. Satisfactory results were obtained by the participants. Let's look at two results in particular. The two blue curves were obtained assuming that the sources were either in a duct (solid line) or in free field (dashed line). At high frequencies the two solutions overlap. At low frequencies they diverge slightly. In the solution calculated for the duct case, we can see peaks that arise when a new acoustic mode is cut-on. These peaks can also be seen in the experimental results. The dotted red curve shows the solution found using a cascade model in combination with a duct. The difference is most pronounced at low frequencies. Other differences between the results are due to the choice of model used to calculate the unsteady lift response.

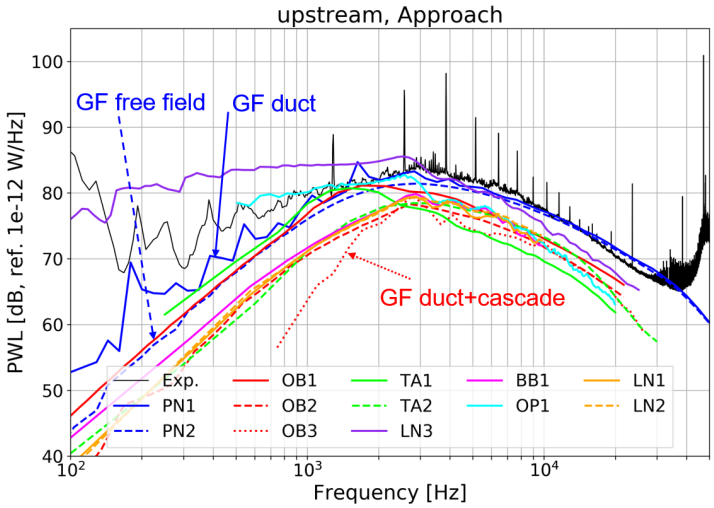


Figure 14: Benchmark results for the prediction of fan broadband noise (Guérin et al. (2020)) (CC BY 4.0).

5.1.4 Source ranking

In this final section we look at the ranking between the sources. The first result in Fig. 15 shows the directivity of the tonal noise compared with that of the broadband noise produced by the turbulence past the trailing edge. In this example, the tonal noise is largely dominant over a wide portion of the directivity. Only at the lowest and highest angles could the trailing-edge noise be audible. In general, broadband noise consisting of a full modal spectrum does not follow the same trends as tonal noise. As shown by

Akiwate et al. (2024), the contribution of tonal noise varies greatly as a function of the operating point and the number of blades.

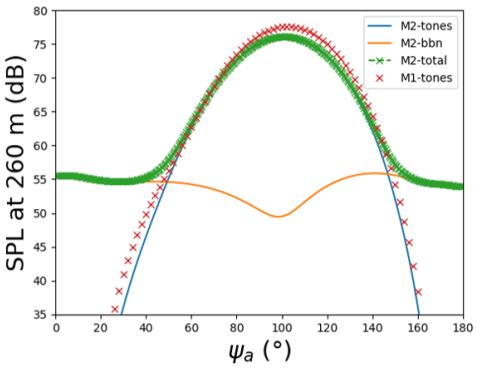


Figure 15: Relative contribution of propeller broadband noise at takeoff (Copyright by Guérin, Tormen (2021). Reproduced with permission.).

The second example deals with two noise spectra emitted at take-off by two turbofans of different design (see Fig. 16). These fans differ, among other things, in their total pressure ratio. The first is supersonic at the tip of the rotor blade, while the other remains subsonic. This prediction illustrates the extent to which the acoustic signature can change when design parameters are changed.

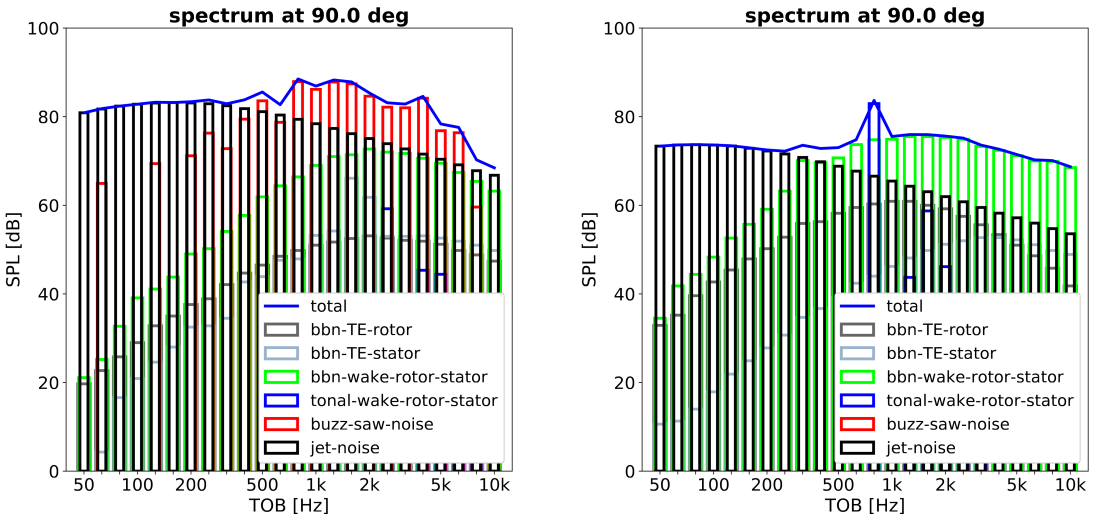


Figure 16: One-third octave band spectra at take-off simulated for two fans with different design parameters: (left) $FPR_{des} = 1.47$, $M_{trel,des} = 1.28$, $D = 1.9\ m$, $(B, V) = (22, 54)$; (right) $FPR_{des} = 1.28$, $M_{trel,des} = 0.89$, $D = 2.7\ m$, $(B, V) = (18, 51)$ (Copyright by Guérin, Moreau, Meier zu Ummeln, Staggat (2021). Reproduced with permission.)

6 Summary

The aim of this course was to show how the noise emitted by a propeller and a fan is different in some ways and similar in others. The target application was conventional commercial aviation.

In the introduction we explained that the use of a turboprop and a turbofan do not meet the same needs. If the number of passengers is small and there is no need for top speed, the use of a propeller is preferable because the propulsion efficiency is much better. However, there are speed and size limits beyond which the use of a turbofan is the only feasible and meaningful solution.

Due to the inherent differences between a fan and a propeller, it is virtually impossible to create an application case where the use of a fan or a propeller are two perfectly equivalent options. Compromises will have to be made in one or other of the specifications. The best option can only be determined by optimising the aircraft as a whole. Acoustics is rarely the primary factor in the design, and the acoustician must accommodate the choices made upstream.

Fans and propellers are both rotating machines. However, they are designed to achieve different operational objectives. The presence of a nacelle and, in the case of the fan, a stator downstream of the rotor is a major difference between the two configurations. But these are not the only differences. The blades also have very different characteristics in terms of solidity and number of blades, both of which are greater in the case of the fan. In addition, high-speed propellers require a system to vary the pitch angle. In terms of aerodynamic performance, a fan remains efficient at supersonic speeds, which is not the case with a propeller. In the absence of a nacelle, the upstream axial Mach of the propeller is imposed by its flight speed. In the case of the fan, this is a design variable as the nacelle regulates the upstream flow.

The rotor noise mechanisms of propellers and fans are the same in both cases. Unlike a propeller, a fan can operate in the supersonic regime, giving rise to the so-called buzzsaw noise. Furthermore, in the case of the fan, the source associated with the rotor–stator interaction is very important, especially in the subsonic regime.

The two analytical solutions derived for the free-field and in-duct Green's functions have shown that there is an approximate frequency below which a spinning mode radiates with low efficiency. For a fan, there is an additional sharp cut-off condition, which explains the exponential decrease in rotor-locked tones at subsonic speeds. We have also explained that transmission effects through the rotor blades are important, especially at high rotor speeds.

Fans and propellers produce both tonal and broadband noise. The noise emitted by the propeller has a significantly lower frequency due to the smaller number of blades and lower speed. Similarly, the amplitude of the sources and their ranking are not the same, which affects the balance between tonal and broadband noise. In general, this can vary considerably depending on the design parameters and the operating point.

7 Related topics

In this study, we have considered the noise emitted by the fan and rotor in an isolated configuration and under the condition of perfect axial flow. Installation effects due to the attachment of the engine to the aircraft wing and the incidence of upstream flow have not been considered. For a fan, the presence of the bifurcation, which is the extension of the pylon in the bypass, can lead to a slight increase in noise. It also leads to a redistribution of the modal content. It can even have an effect on buzzsaw noise (Holewa et al. (2014)). For a propeller, the interaction between the propeller and the wing is a major source of noise. Two types of mechanisms need to be considered: i) the interaction of the propeller wake on the wing and ii) the interaction of the wing potential field on the propeller. Studies have shown that at low speeds these sources can dominate over isolated rotor noise. At high speeds, the relative contribution of interaction noise tends to decrease in favour of rotor self-noise. The propeller is also sensitive to the incidence of the engine axis relative to the direction of flight. In the case of the fan, the nacelle straightens the flow ahead of the fan and helps to mitigate the effect.

The overall noise of a propeller can be effectively reduced by reducing its speed and/or adding more blades. This may have a cost in terms of efficiency and propeller size. At high speeds, sweeping aft is a way of delaying the formation of shocks while creating radial interference that are acoustically beneficial as shown by Hanson (1980).

There are a number of ways of reducing fan noise. Firstly, by modifying the design parameters such as the loading and rotation speed of the rotor (see Jaron et al. (2021)). Significant results can also be achieved by selecting the appropriate blade and vane counts to trigger only acoustic modes that are cut-off. By playing with the axial (sweep) and tangential (lean) position of the leading edge of the stator vanes, it is possible to reduce the tonal interaction noise by favouring the radial interference as shown by Guérin and Moreau (2010). Reducing the number of stator vanes reduces broadband noise at medium and high frequencies. As with a propeller, radial variation of the leading edge contour of the rotor blades can help to reduce the amplitude of the shocks. The use of liner is reserved for fan (see ray-based approach by Moreau et al. (2009)). It is a very effective way of reducing their noise.

There is a growing interest in flying with electrically driven engines in the context of regional mobility. The majority of scenarios are for open rotors. As shown for example in the EU projects IMOTHEP by Guérin and Tormen (2023) and ENODISE by Lade et al. (2024), there are two effects on noise that need to be considered. The pure acoustic interference between the rotors, which gives rise to complex acoustic directivity patterns, and the aerodynamic interaction between adjacent propellers, which can become significant when the spacing between the propeller tips is small. In this respect, shrouded rotors may be less sensitive.

8 Acknowledgments

The preparation of this lecture was supported by the EU's Horizon 2020 program under the ENODISE project GA No. 860103.

The results are based on working with many persons over the last 20 years. Special

thanks go to Antoine Moreau, as some of the most important results have been achieved either by him or in collaboration with him.

The photos in Fig. 1 were taken by Tobias Lade during ILA 2024. They are free of use.

References

Akiwate, D., Joseph, P., Parry, A., and Paruchuri, C. (2024). On the balance between the tonal and broadband noise of isolated propellers. *International Journal of Aeroacoustics*, 23(1-2):122–153.

Amiet, R. (1975). Acoustic radiation from an airfoil in a turbulent stream. *J. Sound. Vib.*, 41(4):407–420.

Chapman, C. (1994). Sound radiation from a cylindrical duct. part 1. ray structure of the duct modes and the external field. *J. Fluid Mech.*, 281:289–311.

Cheong, C., Joseph, P., and Lee, S. (2006). High frequency formulation for the acoustic power spectrum due to cascade-turbulence interaction. *The Journal of the Acoustical Society of America*, 119(1):108–122.

Goldstein, M. (1976). *Aeroacoustics*. McGraw-Hill.

Guérin, S. and Moreau, A. (2010). Accounting for sweep and lean in the design-to-noise of rotor–stator stages. Berlin, Germany. DAGA 2010 Conference.

Guérin, S. and Tormen, D. (2023). A constribution to the investigation of acoustic interferences in aircraft distributed propulsion. *CEAS Aeronautical Journal*, 14:965–982.

Guérin, S. (2017). Farfield radiation of induct-cutoff pressure waves. In *23rd AIAA/CEAS Aeroacoustics Conference, 2017*.

Guérin, S., Kissner, C. A., Seeler, P., Balzquez, R., Carrasco Larana, P., de Laborderie, H., Lewis, D., Paruchuri, C., Polacsek, C., and Thisse, J. (2020). ACAT1 benchmark of RANS-informed analytical methods for fan broadband noise prediction: Part II - influence of the acoustic models. *Acoustics*, 2:617–649.

Hanson, D. B. (1980). Influence of propeller design parametres on far-field harmonic noise in forward flight. *AIAA Journal*, 18(11):1313–1319.

Holewa, A., Weckmüller, C., and Guérin, S. (2014). Impact of by-pass bifurcations on fan noise. *Journal of Propulsion and Power*, 30(1):143–152.

Jaron, R., Moreau, A., Guérin, S., Enghardt, L., Lengyel, T., Otten, T., and Nicke, E. (2021). Multidisciplinary design optimization of a low-noise and efficient next-generation aero-engine fan. *ASME Journal of Turbomachinery*, 144(1):011004.

Lade, T., Guérin, S., A., Z., and de Prenter F. (2024). Analysis of acoustic interference in multi-rotor propulsion. Hannover, Germany. DAGA 2024 Conference.

Moreau, A. (2017). *A unified analytical approach for the acoustic conceptual design of fans of modern aero-engines*. Phd thesis, Technische Universität Berlin.

Moreau, A. (2020). Acoustic shielding in a fan stage predicted with two fast analytical models. Hannover, Germany. DAGA 2020 Conference.

Moreau, A. and Guérin, S. (2011). Similarities of the in-duct and free-field formulations in rotor noise problems. Portland, USA. 17th AIAA/CEAS Aeroacoustics Conference. AIAA-2011-2759.

Moreau, A., Guérin, S., and Busse, S. (2009). A method based on the ray structure of acoustic modes for predicting the liner performance in annular ducts with flow. Rotterdam, The Netherlands. NAG/DAGA 2009 Conference.

Rice, E., Heidmann, M., and Sofrin, T. (1979). Modal propagation angles in a cylindrical duct with flow and their relation to sound radiation. New Orleans (USA). 17th Aerospace Sciences Meeting. AIAA-79-0183.

Sears, W. (1941). Some aspects of non-stationary airfoil theory and its practical applications. *J. Aeronaut. Sci.*, 8(3):104–108.

Spakovszky, Z. (2007). Thermodynamics and propulsion. https://web.mit.edu/16.unified/www/FALL/thermodynamics/notes/node86.html.

Tyler, J. and Sofrin, T. (1962). Axial flow compressor noise studies. *SAE Transactions*, 70:309–332.